



A12 report

Katie Ferraby, University of Liverpool, England

September 8th 2021

In this project, there were three smaller projects. The aim of the first project was to investigate a XUV spectrum and the aim of the second and third projects was to investigate the function of a two-sided spectrometer. Properties of both the ions and electrons produced by the spectrometer were analysed. In project 1, a relationship between position and photon energy was found and used to convert intensity from a function of position to a function of energy. Unknown molecular samples were identified using a conversion from signal-time of flight graphs to mass spectra in project 2 and then analysis of the mass peaks and image files of electron positions on a detector screen were successfully converted into spectral intensity-kinetic energy graphs and kinetic energy-time delay graphs in project 3. Each project was successful; however, further tests are required to validate the physical results obtained in project 1 for the fitted values in the position-energy relationship equation as they were not the size expected and the fit function could have been improved by using another parametrisation.

Contents:

1. Introduction.....	2
2. Project 1.....	2-6
2.1 Theory.....	2-3
2.2 Method.....	3
2.3 Results.....	4
2.4 Discussion.....	4-6
3. Project 2.....	6-10
3.1 Theory.....	6
3.2 Method.....	6-7
3.3 Results.....	7-8
3.4 Discussion.....	8-10
4. Project 3.....	10-13
4.1 Theory.....	10
4.2 Method.....	10-11
4.3 Results.....	11-12
4.4 Discussion.....	12-13
5. Conclusion.....	13-14
6. Bibliography	14
7. Appendices.....	14-15

Introduction:

The first project investigates a XUV photon spectrometer, and the later projects investigate a two-sided spectrometer's dual analysis of electrons and ions.

IR ("infrared") light is split into two beams and travels down two different paths. One of the beams is analysed as it undergoes high harmonic generation (HHG) and through an Aluminium filter, before recombination. That beam is passed through a diffraction grating and measurements are taken. We received this data, and our project was to analyse this dataset.

The second and third experiments can both be conducted with the same spectrometer. Gas is injected into the spectrometer and when it is ionised, the ions move to one side and the emitted electrons move to the other side because they have opposite charges and so are attracted to their oppositely charged plates on either side. The second project follows the ions and converts their signal-time of flight recordings to a mass spectrum while the third project follows the electrons and converts the electron positions on a detector screen to readings of kinetic energy, time delay and signal.

The techniques demonstrated in project 3 are extremely useful. A beam splitter splits light and then the two beams travel down individual paths before recombining at a later point. Afterwards, one of the beams interact with the sample ('the pump') and then after a time delay, the other beam ('the probe') interacts with the sample.

In project 1, one can measure the XUV light which is the 'pump' and project 3's scans use the pump-probe scan capability. The probe is measured after the interaction. In one case, the pump can excite the sample and so when the probe is measured, information can be found out about the de-excitation process and one can learn about the motion of electrons.

This 'pump-probe spectroscopy' method is excellent because time resolution now depends on the laser pulse duration and not the detector and so can be shorter than picoseconds and the movement of a mirror. [1]

Mass spectrometry has many uses in many industries. The molecules in samples can be determined and the molecules that sample fragments into can be identified and so the method in project 2 is useful for checking for sample contamination, forensic analysis, and many types of drug testing. [2]

Project 3 is useful for understanding more about the states close to the ionisation threshold and how different lights interact in a sample.

Project 1:

Theory:

When atoms are exposed to laser light, high harmonic generation (HHG) can happen. An electron undergoes quantum tunnelling and after the emission, the electron is accelerated by the laser's electric field and so gains kinetic energy. The electron then turns back towards the ion and is reabsorbed. As the electron gained energy after leaving the atom, the atom now has increased energy after the recombination. This process is high harmonic generation [3]. The atom emits radiation with integer multiples of the laser's frequency – these are harmonic orders.

Adjacent harmonic peaks are separated by $2\omega_0$, where ω_0 is the fundamental frequency, because the HHG process occurs twice every optical cycle of the laser's field and because the direction the electron travels to return to the ion alternates, only the odd harmonic orders are produced.

As seen in figure 1 below, L is the distance from the diffraction grating to the screen and Y is the distance to the first peak plus an offset.

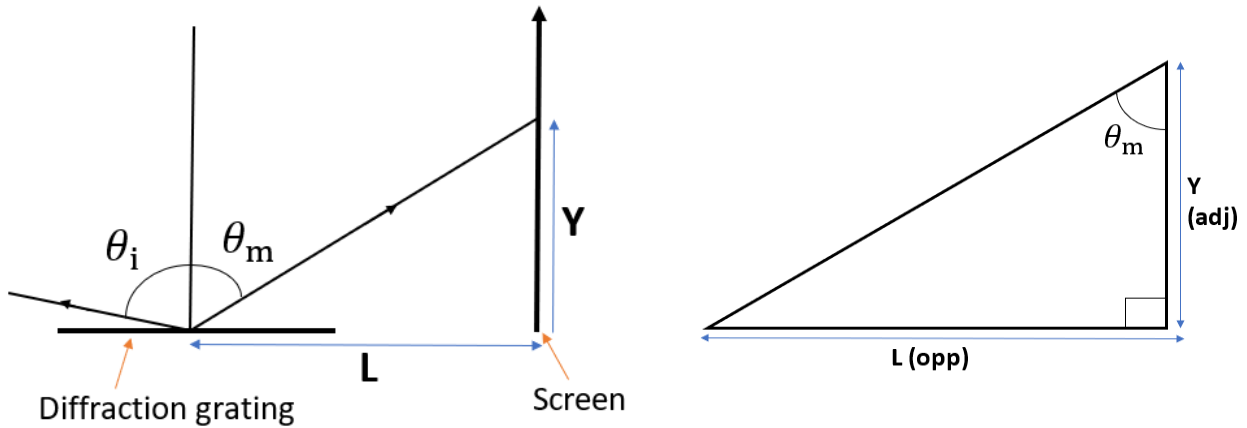


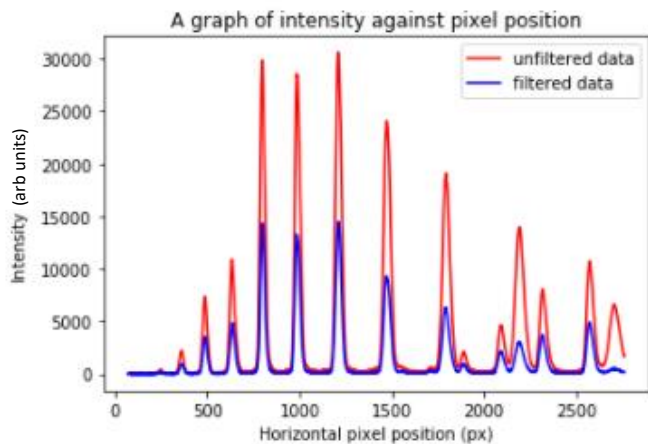
Figure 1: This is a diagram showing light incident on a diffraction grating and then being diffracted and detected on a screen. The smaller triangle is a rearrangement of the bigger diagram and shows the angle θ_m . By rearranging the first diagram, the calculations are simplified. The light is from one of the light rays from the beamline after undergoing HHG and travelling through an Al filter.

$$y = \frac{L}{\tan\left(\sin^{-1}\left(\frac{1}{d}\left(A - \frac{mhc}{E}\right)\right)\right)} - y_0 \quad (1)$$

Equation 1 was derived from figure 1 and shows the relationship between pixel position and photon energy. The constants L , d (grating spacing), $A = d \sin \theta_i$ and y_0 are unknown and must be found for conversions between the two variables, y – pixel position - and E – photon energy.

Method:

Two datasets of intensity and pixel position were given. Intensity is a function of position and is detected along the y -axis in figure 1 as the camera is behind the screen. The two datasets were plotted on the same graph and intensity was plotted against pixel position. One dataset was for unfiltered values, measurements taken before the light travelled through the Aluminium filter and the other dataset was for filtered values, for measurements taken after the light travelled through the Aluminium filter. The plot is shown below.



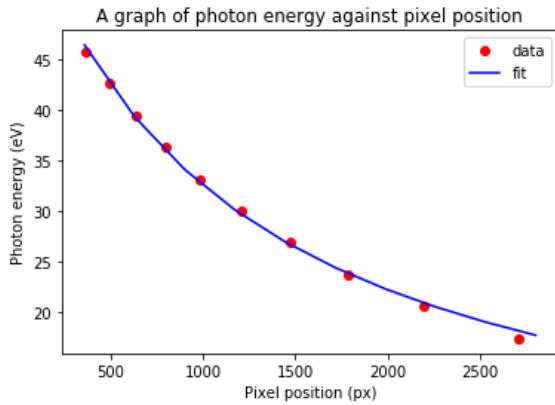
Graph 1: This is a graph of intensity against pixel position – a plot of the original file for project 1.

The peak positions and their heights were recorded, and the transmission fraction (unfiltered peak/filtered peak height) of each peak was calculated and an aluminium filter transmission graph can be used to find the energy values corresponding to the fractions. By comparing these graph energies against trial and error energy values of $n\hbar\omega_0$, the matches can reveal which harmonic orders correspond to which peak. The fundamental energy was calculated by finding the wavelength of the peak of the spectrum of the driving IR laser and converting it into an energy value. The energy was 1.58eV.

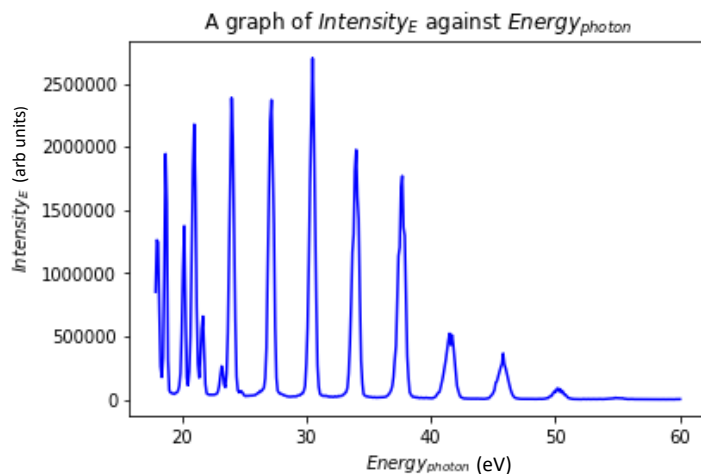
The main exercise of project 1 was to find a relationship between pixel position and photon energy to enable a conversion between the variables and to create a spectrum with intensity shown for equally spaced energy bins. The relationship is shown in equation 1. The constants in the relationship must be fitted using a fit function and are displayed in the results discussion.

After this, a graph of intensity as a function of energy is plotted against photon energy. Intensity is a function of pixel position, and these values are not equal to the intensity values when intensity is a function of photon energy. The function that converts pixel position into photon energies is not a linear function, the derivative of the function varies, and so one cannot directly convert an intensity-pixel position graph to an intensity_{energy}-photon energy graph as the 'area under the curve' must be conserved. Because of this issue, the intensity values must be converted into a function of energy. This is done by converting an array of evenly spaced energy values into pixel positions - these become limits - and then the corresponding intensity values are found and the intensity values between two adjacent limits are added together using a 'for loop'.

Results:



Graph 2: A graph of photon energy against pixel position shows the agreement between the data and fit function, equation 1. From the curve fit, the L , d , A and y_0 constants were found to be: 1.65×10^5 px, 4.49×10^{-3} m, 1.18×10^{-4} m and 6.25×10^6 px respectively.



Graph 3: A graph of intensity as a function of energy plotted against photon energy. The energy scale is correct for the 1st order peaks.

Discussion:

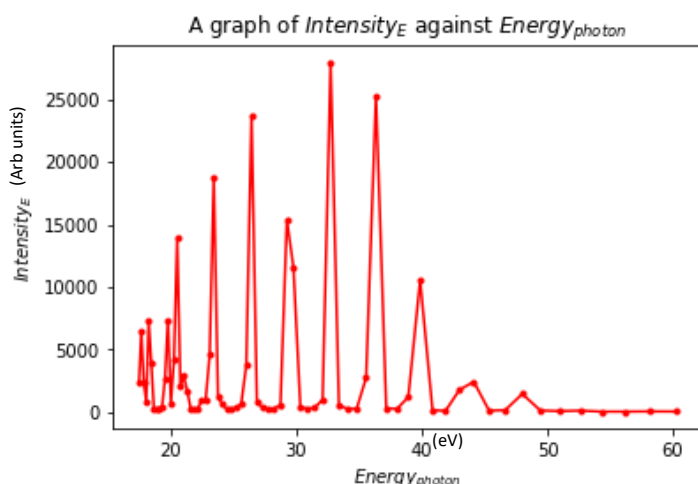
The graph of transmission fraction against photon energy in the aluminium filter was produced. The transmission axis shows what fraction of photons are absorbed by the filter and this absorption is why the peak heights in graph 1 for the unfiltered and filtered data are different heights – the filtered peaks are smaller because there are less photons per second contributing to the intensity of the light after the filter.

As seen in graph 2, the fit agrees well with the earlier data points between 500 and 2000 px but the fit starts to diverge from the data points past 2000 px and the fit does not go through the last data point. The value of d , the grating period, was 4.49×10^{-3} m which is very big for diffraction gratings and a value closer to 10^{-6} m was expected. The value of $\theta_i (= \sin^{-1}(\frac{A}{d}))$ was also extremely small at 1.5 degrees and a value greater than 80 degrees was expected. The initial estimates for L , d , A and y_0 were 25 px, 7×10^{-7} m, 5.84×10^{-8} m and 50 px respectively and then the produced fit values were used as the initial guess to increase fit accuracy to produce the final fit values of 1.65×10^5 px, 4.39×10^{-3} m, 1.18×10^{-4} m and 6.25×10^6 px respectively. The initial guesses led the fitter astray and so even though the initial guesses were changed to improve the accuracy, it was in vain because the first fit had already led the fitter astray.

As the fit did not go through all the data points and the fit values were not as expected, a future experiment could be carried out to determine if the derived equation is correct or if there is a physical effect or term that was not considered. The fit could also be refined and use $d \sin \theta_i$ instead of A because then the sine term limits the values θ_i can take and so the optimizer will be constrained to physically meaningful choices rather than parameters just being chosen for making the correct shape. A (roughly) correct shape of the curve is all that is needed to be able to convert the spectrum and so graph 3 only has minor errors even if the fitted parameters are not optimal.

As seen in graph 3, the trend of the graph, the relative height of the peaks, is reversed from the original intensity-pixel position graph. This is because the peaks in the original graph increase in energy from right to left and in the intensity-photon energy graph, energy increases from left to right.

If the values are directly converted without using a 'for loop', the graph produced is shown below:



Graph 4: This is a graph of intensity as a function of photon energy. The graph is an alternative version of graph 3 where the intensity values were directly converted into a function of energy, which is an incorrect method.

In this graph, the chosen points which are equally spaced in position (pixels) end up closer spaced for low energies than for high energies. Furthermore, the shape of the graph is different to the shape of the original intensity-position graph, most noticeably the peak at 30 eV has dramatically decreased and the peak at 40 eV has increased.

There was a debate whether the harmonic peaks should start at the 9th order or 11th order. For the lowest energy peak, the energy corresponding to its transmission fraction was found on the Aluminium filter graph and odd integers multiplied by the fundamental energy were trialed to determine what 'n' gave an energy value closest to the transmission fraction's energy. The closest value was either from n=9 or n=11. Neither choice made a good fit of the step and plateau shape expected: the peaks have a spacing of $2\omega_0$ and so once n=9 is chosen, the harmonic orders of the peaks go up in odd integers from 9 to 27 or once n=11 is chosen, the orders go up in odd integers from 11 to 29. These harmonic labels don't give a filter graph with the correct increase and plateau. The shape is incorrect for both n=9 or n=11.

N=11 gave a better fit for the photon energy-pixel position graph. By eye, the last two points for the n=9 graph diverged much more than the n=11 graph but the RMS errors could have been plotted for the n=9 and n=11 graphs to determine mathematically which had the best fit. Overall, n=11 gave better results and so was chosen to be the lowest harmonic peak.

Project 2:

Theory:

For all of the signal-time of flight graphs - and mass spectra – the height of the peaks correspond to how abundant a molecule is amongst the created ions– the higher a peak is, the more abundant the molecule. For the air sample in directory 1, the composition percentages of air are known and so the molecules that were most abundant were used for calibration testing as they were the easier to match to the time peaks.

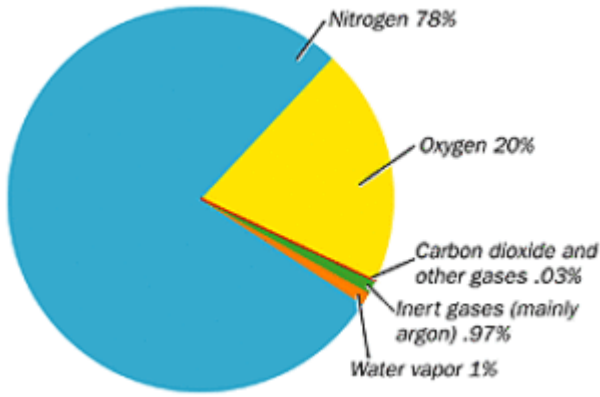
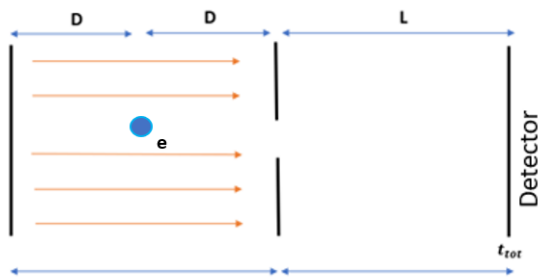


Figure 2: This figure shows the composition of air as percentages. Nitrogen makes up most of atmospheric air, followed by oxygen and water vapour. [4]

There is a chosen offset in the experiment's time-axis because it takes time for recording to begin and so one must be careful with the early peaks as they may not correspond to a molecule, they may correspond to the 'cross-talk' from the trigger pulse for a camera for an electron image and from electrons colliding.

Method:



D is the distance from the electron's initial position to the end of the electric field region. L is the length of the non-electric field region. The blue circle represents an electron in the set-up. t_{tot} is the time taken for the electron to reach the detector after it is emitted.

If a charged particle with an initial velocity travels through an electric field region and then continues to travel through a non-electric field region until it reaches a detector, the relationship between its time of flight and mass is derived as:

$$t_{tot} = \left(\frac{m}{q}\right)^{\frac{1}{2}} \left(\frac{2D+L}{V}\right)^{\frac{1}{2}} \quad : \quad t \propto m^{\frac{1}{2}} \quad (2)$$

Where m is the mass of the molecule, q is the charge of the molecule, D is the distance between where the particle started and the end of the electric-field region, L is the full width of the non-electric field region and V is the potential of the metal plates.

The signal-time of flight files must be calibrated to calculate the conversion between time and mass/charge values. The charge is assumed to be +1e because the injected gases are all neutral and when they're ionised, they lose one electron and so have a charge of +1e and so the mass/charge ratio dependence becomes a dependence on mass only.

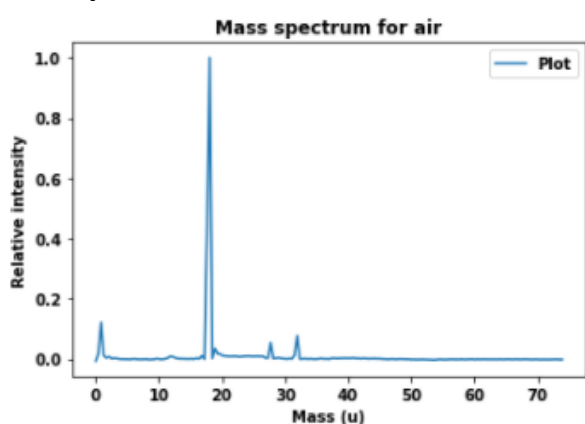
The data files were grouped in directories where each directory needs its own calibration as the datasets were recorded under different circumstances. The calibration function was provided values for some peaks – its time of flight value and our guessed potential molecular mass. In directory 1, the molecules that made up air were trialled; in directory 2, molecules making up N2 and air were

trialled and in directory 3, the molecules that made up the list of possible samples were trialled. Once the calibration returns the smallest deviation possible for the file, the calibration is applied to all the files and for each file, a mass spectrum graph can be plotted - signal against mass– using equation 2.

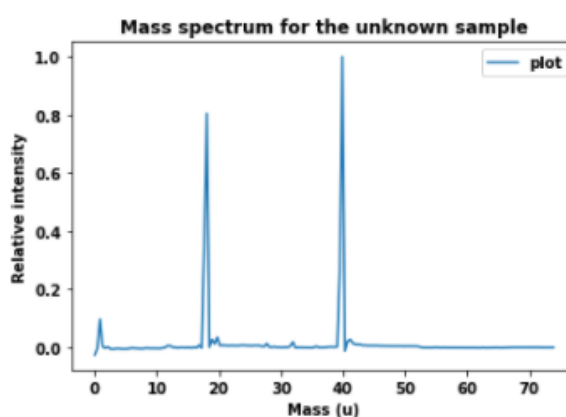
The mass peaks correspond to different molecules and so the molecules that make up a sample can be identified from this set-up and method. For directory 1, by finding the molecules corresponding to the peaks, the unknown sample or peak can be identified. For directory 3, the produced mass spectra can be compared to the reference mass spectra and from the comparison, the samples can be identified, and the lighter ions present can be determined as well.

Results:

Directory 1:



Graph 5: This is the mass spectra graph corresponding to the 'air' sample. It was produced by calibrating the air sample and then converting the time of flight values to mass values.

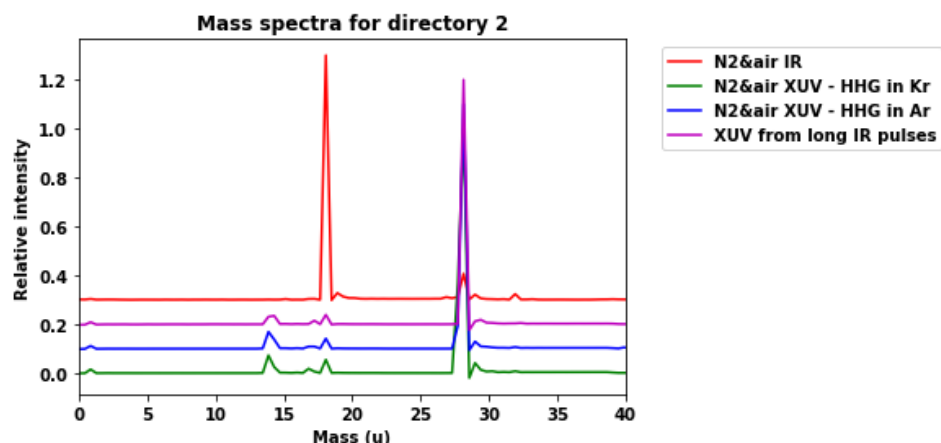


Graph 6: This is the mass spectra graph for the unknown sample, calculated using the calibration from the air sample.

Mass peak (integer)	Molecule (substance)
1 u	Hydrogen atom
18 u	Water
20 u	Neon atom
28 u	Nitrogen
32 u	Oxygen
36 u	Argon-36
40 u	Argon-40

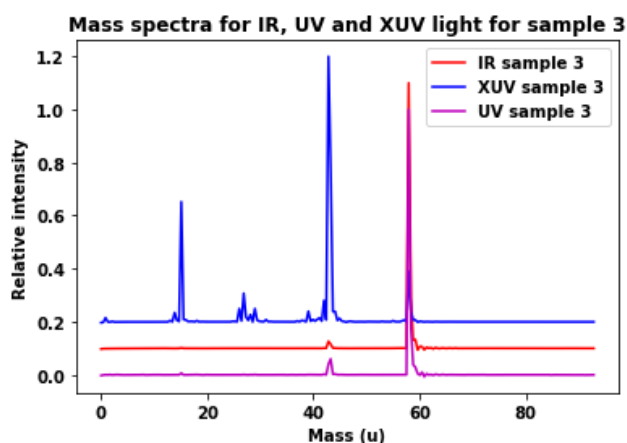
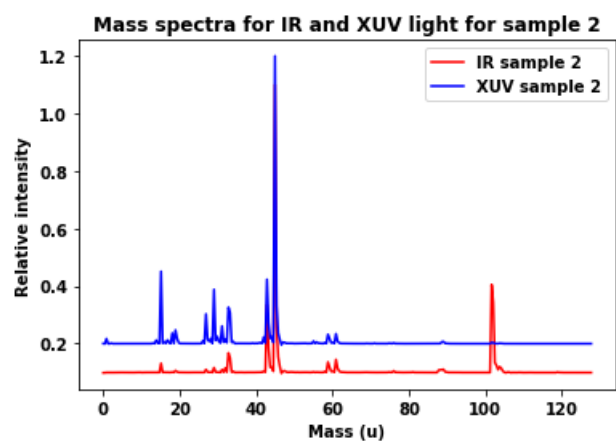
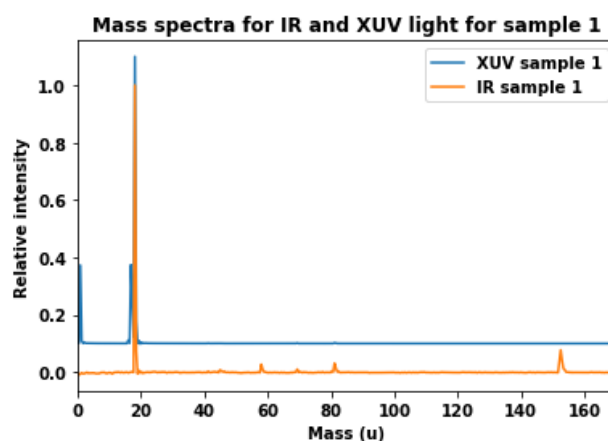
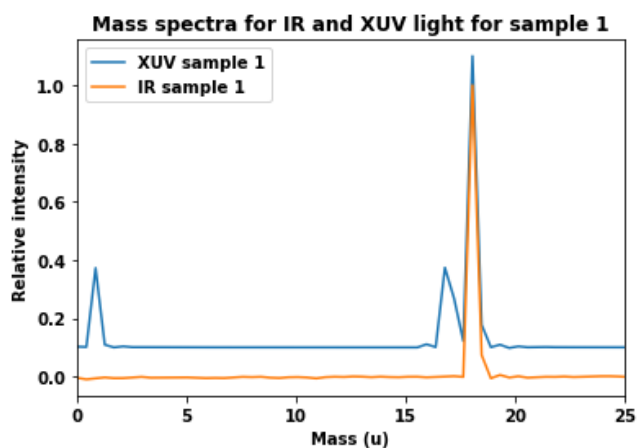
Table 1: This is a table of the mass peaks and their corresponding molecules for the unknown sample. The unknown peak was Argon at 40u.

Directory 2:



Graph 7: This is the mass spectra graph for all the directory 2 files. It was produced by calibrating the 'N2&air IR 036.h5' file and then then applying the calibration and conversion to all the files. The graphs were all given a vertical offset so the individual mass spectra could be seen.

Directory 3:



Graphs 8.1, 8.2, 8.3 and 8.4: Graph 8.1 is a zoom-in of graph 8.2, focusing on the fragment peaks. Graphs 8.2, 8.3 and 8.4 are the mass spectra produced for the sample 1, 2 and 3 files, with a slight vertical offset for the files so the plots can be individually seen and compared.

Sample	Fragment 1	Fragment 2	Fragment 3
Sample 1 – water	1 u - hydrogen	17 u - OH	18 u – water
Sample 2 – methyl lactate	29 u - CHO	43 u – C ₂ H ₃ O	45 u – C ₂ H ₅ O
Sample 3 – acetone	15 u – CH ₃ ⁺	43 u - C ₂ H ₃ O	58 u - acetone

Table 2: This is a table of each sample in directory 3 with 3 fragments identified in each sample.

Discussion:

When molecules are ionised, they may not be stable and therefore they break apart and so there are some peaks present that were not initially expected. For example, water can break apart into hydrogen and OH and so there are peaks at 1u and 17u even though these two do not make up a significant percentage of air.

In sample 1 for directory 3, peaks with different strengths are seen for the same molecule – for example, in the IR file, water has a high peak but in the UV file, water has a low peak, and this is because certain light finds it harder to ionise certain molecules and so the peak strengths change as more or less ionisation occurs.

Larger peaks are seen in the IR light files, but smaller peaks are rarely seen, and the reverse is true for the UV light files. IR photons have less energy per photon than UV light and so the sample can absorb more energy at once from a UV photon. For IR light to match the energy absorbed, multiple IR photons must be absorbed at the same time, but as the number of photons needed increases, the likelihood of all the photons being absorbed simultaneously decreases. A certain amount of energy is needed for ionisation and there will be less excess energy from IR photon absorption than UV photon absorption and this excess is used to break bonds in the molecule. Because of the smaller excess for IR light, only smaller fragments can split from the parent molecule as less bonds can be broken and so peaks are seen for the larger remaining molecules and for UV light, larger fragments can split off because there is more excess energy and so peaks are seen for the smaller remaining molecules. IR light favours molecules with low ionisation energy because it is easier to produce the required ionisation energy. [5]

The calibration could have been done with only two peaks; however, the calibration is more accurate when done with more peaks because small errors can average out when there are more datapoints to fit. The calibration has two parameters so when given more than 2 points, the fit is not exact, and the magnitude of the deviations can be used to choose between alternative assignments. The closer the deviation is to zero, the better the fit has performed. Issues that would cause a larger deviation are the wrong molecules being attributed to the peaks, or the peak positions being incorrectly recorded, however, the deviation give some insight into the fit and its validity.

Argon-40 was found to be the unknown peak in the unknown sample of directory 1. Hydrogen, water, neon, nitrogen, oxygen, and argon-36 were found to be other mass peaks.

A complication that can come up is what molecule an unknown peak corresponds to – for example, a peak appeared at 35.91u for the unknown sample in directory 1 and this can potentially correspond to many molecules as they have similar masses. A potential way to discern which molecule corresponds to the peak is to consider the isotopes of the present molecules. Argon-40 is present in the sample and so the other isotopes of argon must also present, but they may not produce strong peaks due to the lack of abundance. Ar-36, Ar-38, Ar-40 are all present with an abundance of 0.33%, 0.063% and 99.6% respectively of all argon present. As all the isotopes must be considered, this explains that Argon-36 corresponds to the 35.91u peak and not, for example, Hydrogen Chloride with a mass of 35.98u.

In directory 2, the XUV light (“extreme ultraviolet light”) favours the mass spectra peaks at 1u, 14u, 17u and 28u which correspond to hydrogen, nitrogen, OH and N₂ and the IR light favours the peaks at 2u, 18u and 32u which correspond to H₂, water and oxygen. The lights favour these peaks as in their respective graphs, these molecules have the greatest peaks and so, the greatest intensity.

The XUV light files for directory 2 show no peaks after 75u on the mass spectrum but in the IR light file, peaks are seen after this point and so IR light is better at finding contaminants, finding the heavy, high mass hydrocarbons in the sample. This is because hydrocarbons have a low ionisation energy and so they are favoured by IR light. Another sample is the 152u peak seen only in the IR file for sample 1 for directory 3 – it is a residual of fenchone from another experiment and is a contaminant in this sample.

The samples in directory 3 were identified by comparing the reference mass spectra from NIST Chemistry webbook to the mass spectra produced for each sample. Similar peak groupings and peak masses were analysed and compared until the mass spectra that best matched the produced spectra were found. As seen in graph 8.2, 8.3 and 8.4, XUV light gives smaller fragments and IR hardly breaks into fragments, but it can see heavy contaminants, for example, the contaminants in sample 1, graphs 8.1 and 8.2.

Project 3:

Theory:

In the spectrometer, the initial velocity influences where the electron ends up being detected. When the electron has an initial velocity, its path through the electric field becomes a parabola and if the velocity has an upwards component, the electron path curves upwards and if it has a downwards component, the path curves downwards. After multiple electrons have been emitted and have travelled to the detector, if the initial speed is randomly directed, the plot of detected electron positions should look like a circle on the detector screen.

$$r^2 \propto \frac{mv_{r0}^2}{2} \quad (3)$$

From equation 3 above, one can see that radius² (r^2) is directly proportional to transverse velocity² (v_{r0}^2). As velocity² is directly proportional to kinetic energy, radius² is directly proportional to the component of kinetic energy in the xy-plane, perpendicular to the axis of spectrometry. This means that the greater the curvature of the electron's path, the more kinetic energy the electron has.

Method:

One of the goals for project 3 was to convert images of the electron positions on the detector to a spectral intensity against kinetic energy spectrum. The xy plane is parallel to the detector's plane.

From equation 3, we can introduce a calibration constant 'c' to convert between the kinetic energy and radius squared.

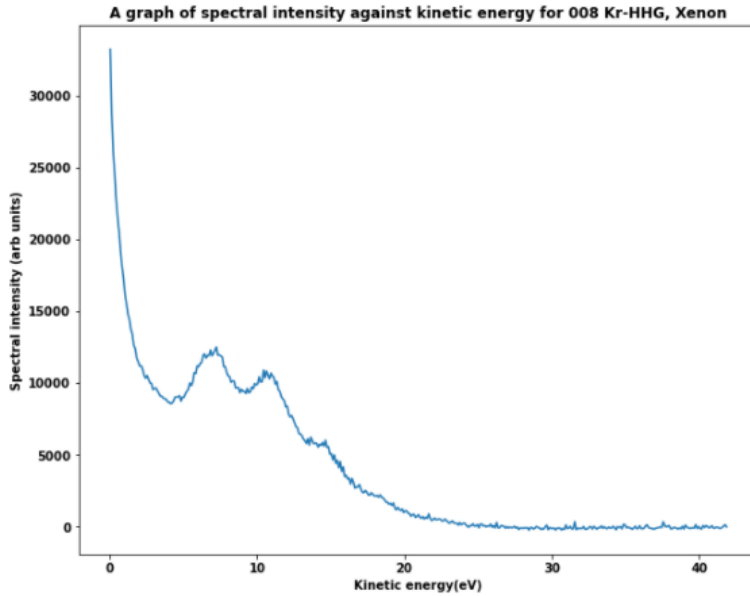
$$\frac{mv_{r0}^2}{2} = cr^2 \quad (4)$$

The constant 'c' depends on the fields' voltages and was given by the supervisor. The calibration depends on when the image was taken and may change between image files. The pixel size depends on the camera set-up and distance and may also vary.

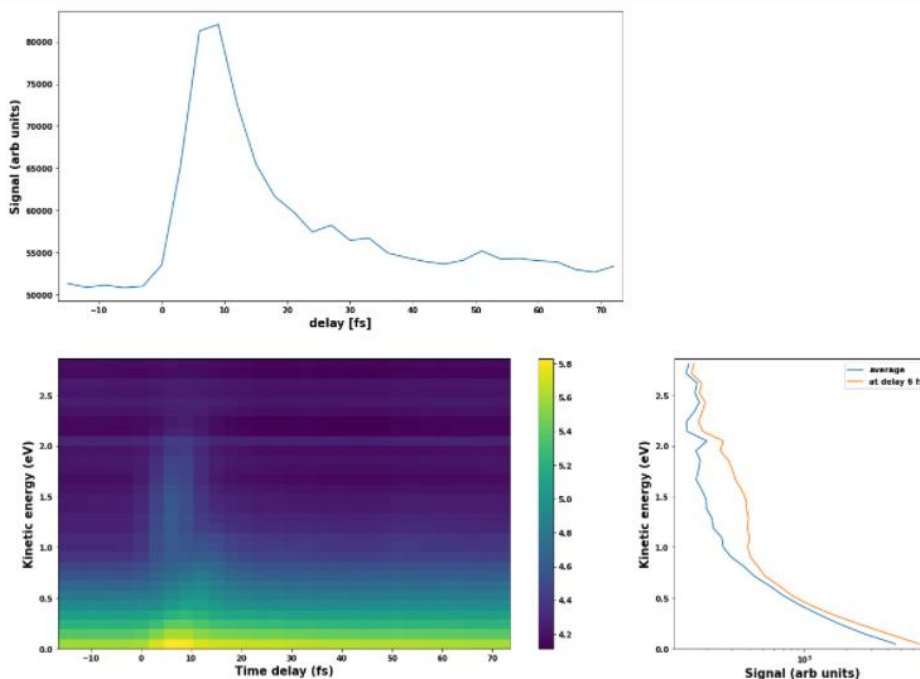
The project extends after the kinetic energy spectra are plotted. The same calibration function with different values is used on files from a UV-pump-IR-probe scan to produce a kinetic energy against time delay graph. From this graph, a signal-time delay graph and kinetic energy against signal graph can be extracted.

To produce a kinetic energy against time delay graph, the central coordinate was determined by looking at one of the files and from this, the other files were calibrated. In a 'for loop', a kinetic energy spectrum is produced, and the time delay is recorded for each image file and then these values can be joined as a matrix and plotted with a colour bar to get the spectrum colour map.

Results:



Graph 9: This is a spectral intensity against kinetic energy graph for the '008 Kr-HHG, Xenon' file.



Graph 10: The bottom left panel is a $\log_{10}(\text{signal}/\text{arb units})$ colourmap of kinetic energy against time delay. The graph above the colourmap is a graph of signal against time delay and the graph to the right of the colourmap is a kinetic energy against $\log_{10}(\text{signal}/\text{arb units})$ graph. These graphs are produced for an acetone sample using a UV-pump and IR-probe.

Discussion:

In the single-laser shot image files, each coloured spot should be an electron on the detector screen but there are some coloured spots which are noise from the camera. Often, if a bright pixel is surrounded by dark pixels, the spot is due to noise. Subtracting a background, minimum energy

value from the file helps remove these noise spots and help differentiate between noise and electron pixels. However, there are different levels of sensitivity in areas of the camera and so some noise may not be fully removed with the background and threshold setting from an area with increased sensitivity – also, weak electrons may be accidentally removed if a too high threshold is set.

For graph 9, each ring in the image corresponds to a peak in the kinetic energy spectrum and the rings further from the central spot increase in energy. The peak at 0 eV is for the central spot and the second peak is for the first bright ring.

Graph 10 shows different aspects and properties of the same scan and shows an example of electron spectroscopy.

UV light is sent to interact with the acetone sample. UV photons can be absorbed by the acetone atoms but not ionise them if they don't transfer enough energy, they may only have enough energy to excite the atoms. Though, for example, 3 UV photons can ionise the atoms, it is more likely for only 2 UV photons to be absorbed and excite the atoms. When this happens, states near the threshold for ionisation are populated.

When the IR light is sent after a delay and IR photons absorbed, in some cases, some states now have enough energy for the atom to be ionised and then the kinetic energy of the emitted photoelectron is recorded.

At 6fs of the uncalibrated delay axis, the UV and IR lights overlap and instead of IR photons being absorbed by states excited by UV light, ionisation could happen because of energy transferred due to a combination of multiple UV and IR photons being simultaneously absorbed. This only works when the pulses overlap, and therefore a peak can be seen at 6 fs.

The colourmap shows intensity as a function of kinetic energy and time delay. There is an offset of 6 fs in the kinetic energy-time delay graph and as the other two graphs are products of the colour map graph, they are also affected by this offset. The calibration isn't perfect because at 0 fs the UV and IR light pulses should overlap but this happens at 6fs.

In the colourmap graph, the colourmap starts at 4.2 and as it is a \log_{10} graph, 4.2 corresponds to $10^{4.2}$. The colourmap starts at this value rather than 0 because there is noise from the camera contributing to the signal. The logarithmic graph also makes it easier to see the light blue peak at around 6 fs delay in the original graph.

The top graph shows signal strength as a function of time-delay and again, shows how the signal strengthens up to a delay of 6 fs when both light pulses interact with the acetone and then weakens at a slower rate. The signal does not return to values as low as those before the peak. The signal increases as more ionisations happen and decreases after the pulses no longer overlap. The decrease is exponential due to some transitions making below-threshold molecules no longer available for ionisation by IR photons.

The graph to the right shows the kinetic energy as a function of signal and shows how signal decreases with kinetic energy. The bulge in the 6fs plot - between 1.0 and 2.0 eV - also corresponds to the peak in the other two graphs. A simplified explanation of the graph on the right is that one can determine how many photons and how many of each kind are needed to be absorbed for a photoelectron to have a certain kinetic energy. IR photons have an energy between 1.5 and 1.7 eV

and UV photons have an energy three times as big and so the energy transferred from a combination of photons can be tested to make a specific kinetic energy reading from the graph.

For example, from this graph, one can assume that 2UV photons and 1 IR photon were absorbed simultaneously when the UV and IR light pulses overlapped. When the energy of these photons are combined and the ionisation energy for acetone is subtracted, the resulting photoelectron kinetic energy is calculated as a range between 0.8 eV and 2.2 eV. There is a range as the IR photons have a range of energies because a broad spectrum is used. As seen on the graph, 0.8 eV is the minimum y-value, and 2.2 eV is the maximum y-value of the bulge and so it is confirmed that this set of photons were absorbed when there was an overlap.

Conclusion:

Overall, the main goal in project 1 was achieved. The relationship between pixel position and photon energy was found and a method to convert intensity from a function of pixel position into a function of photon energy was developed and carried out. The unknown samples in project 2 were found to be water, methyl lactate and acetone and the unknown peak in part 1 was argon. Project 3 showed that a kinetic energy spectrum could be produced from an image file of electron positions on a detector along with a graphs of: energy against time delay, signal against time delay and signal against energy.

The fitted values in project 1 were not expected and are not likely to be correct. The 'd' value for grating spacing is usually closer to a micrometre size and the θ_i value should be greater than 80 degrees. However, the pixel position-photon energy graph had a good fit visually and the intensity-energy graph had the expected shape and peak heights. The calibrations for the directories in project 2 had three well fitted assigned peaks and so the graphs were likely correctly converted and analysed. To improve project 1, the fit for the position-energy graph could be improved by using $d \sin \theta_i$ rather than the arbitrary parameter A. A different equation could also be fitted to determine if the problem with the fitted values were due to the poor initial estimates or due to the equation being incorrect. The calibrations done in part 1 of project 3 could be improved so the spacing between the kinetic energy peaks for the spectral intensity-kinetic energy graph match up with the photon energies used in the sample's ionisation.

Bibliography:

[1] Paschotta, R., 2004. *Time-resolved Spectroscopy*. [Online]

Available at: https://www.rp-photonics.com/time_resolved_spectroscopy.html

[Accessed 29 08 2021].

[2] ThermoFisherScientific, 2006. *Mass Spectrometry Application Areas*. [Online]

Available at: <https://www.thermofisher.com/uk/en/home/industrial/mass-spectrometry/mass-spectrometry-learning-center/mass-spectrometry-applications-area.html>

[Accessed 28 08 2021].

[3] Nisoli, M., 2017. *Attosecond Electron Dynamics in Molecules*. [Online]

Available at: <https://pubmed.ncbi.nlm.nih.gov/28488433/>

[Accessed 03 09 2021].

[4] Toppr, 2013. *Components of Air*. [Online]

Available at: <https://www.toppr.com/guides/science/air-around-us/components-of-air/>

[Accessed 16 08 2021].

[5] Fernandez, M., 2008. *What is light?*. [Online]

Available at: https://ec.europa.eu/health/scientific_committees/opinions_layman/en/energy-saving-lamps/l-2/1-light-electromagnetic-spectrum.htm

[Accessed 18 08 2021].

Appendices:

Appendix A:

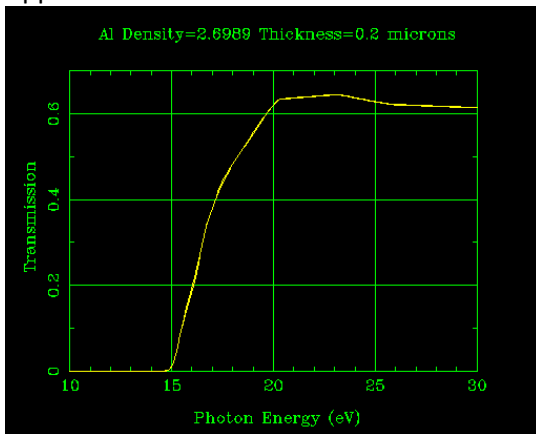
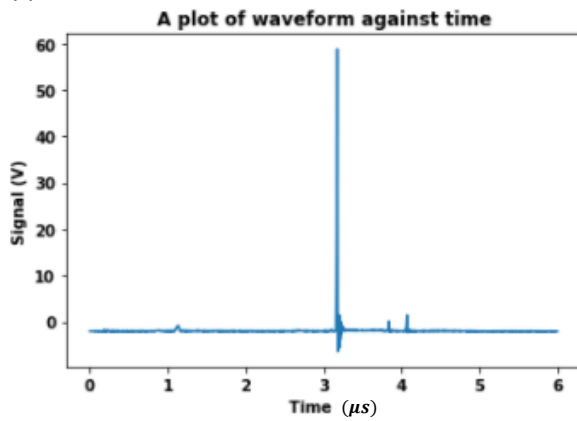


Figure 3: This figure is the reference Aluminium filter graph.

Appendix B:



Graph 11: This is a graph of signal against time of flight. It is an example file given for project 2. This is the file for the 'air' sample.

Appendix C:

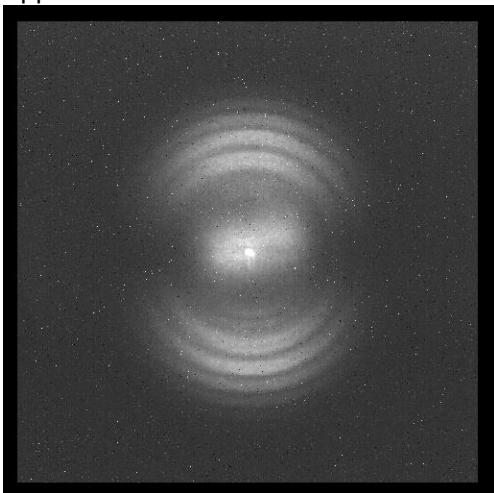


Figure 4: This is an example of the given files for project 3 – it is a photo of electrons' positions on a detector screen. It is from the '008 Kr-HHG, Xe sample.h5' file.